


Article

Experimental balance model adjustment based on force-torque sensors

Santiago Martinez ^{1,†,*} , Juan Miguel Garcia ¹, Juan G. Victores ¹, Alberto Jardon ¹ and Carlos Balaguer ²

¹ Universidad Carlos III de Madrid; scasa@ing.uc3m.es

* Correspondence: scasa@ing.uc3m.es; Tel.: +34-91-624-5997

Academic Editor: name

Version December 31, 2017 submitted to Sensors

Abstract: The computational complexity of humanoid robot balance control is reduced by means of applying simplified kinematics and dynamics models. But these simplifications lead to introduce errors that are added to other inherent electro-mechanic inaccuracies of the robotic system. But linear control systems deal with these inaccuracies if they operate around an specific working point but are less precise if not. This work presents a model improvement based on the Linear Inverted Pendulum Model (LIPM) to be applied in a non-linear control system. The aim is to minimize the control error and reduce robot oscillations for multiple working points. The new model, named Adjusted LIPM, is used to plan the robot behavior against changes in the balance status denoted by the Zero Moment Point (ZMP). Thanks to the use of the information of Force-Torque sensors, an experimental procedure has been applied to characterize the inaccuracies and introduce them in the new model. The experiments have consisted of balance perturbations similar to push-recovery trials, in which step shaped ZMP variations are produced. The results show that the response of the robot against balance perturbations are more precise and the mechanical oscillations are reduced without comprising the robot dynamics

Keywords: Force-Torque sensors, balance control, humanoid robot, simplified models

1. INTRODUCTION

In robotics, the most versatile but complex machines are humanoid robots. Their complex mechanical structure, high number of Degrees of Freedom (DOF) and, control requirements favor the seeking for simplifications that enable the deployment of multiple tasks. Human-like or humanoid robots are designed for working in scenarios in the same way than humans do but they have nowadays very serious limitations performing tasks. For instance, working in manufacturing plants in which heavy parts must be processed, disaster scenarios, service applications, etc. In such situations the need for interaction with the surrounding environment is always present. Humanoid robots, physically similar to human beings, must fulfill a very important requirement: the robot must be able to move around its environment keeping balance.

When a humanoid robot performs tasks and walks through plain, rough or sloped terrains it has to be ensured that the robot will not fall over [1][2]. Even if there are obstacles placed in the robot environment and path re-planing is required [3][4], normal step pattern must be changed always maintaining stability. Furthermore, previous to walking pattern generation, robot joints constraints, dynamic parameters (velocities, accelerations, etc.), and joint torques [5] have to be observed in real time to not overload the system and make the walking task viable.

In the case of human beings presence, unexpected disturbances can appear due to intentional or accidental interactions. In this situation the robot is actuated by an external force and the robot must

34 counteract it to recover its balance status and prevent a falling [6][7]. A more complex situation comes
35 when the robot is carrying an object itself or collaborating with a human [8]. An unknown weight
36 has to be considered and the system model is completely different, taking the object as a part of its
37 body. Each one of these situations lead to the use of one particular model of the robot which takes into
38 account different requirements from the surrounding environment, the mechanical distribution of the
39 robot itself, etc.

40 Their complex mechanical structure, high number of Degrees of Freedom (DOF) and, control
41 requirements favor the seeking for simplified models that enable the deployment of multiple tasks.
42 But the use of these models lead to the amplification of inherent inaccuracies of the humanoid robot
43 system. The concept of 'simplified model' implies the assumption of errors to favor other aspects such
44 as computing velocity, controllability, etc. The simplest model of a humanoid robot used in balance
45 control is the inverted pendulum. It represents the location and movement of the Center of Mass
46 (CoM) of the robot, which pivots around a support base thanks to a rotating joint. Due to its simplicity,
47 its easy to state that many inaccuracies are introduced and system features are omitted. For instance,
48 the location at any time of the CoM depends on the robot posture and may not be coincident with the
49 location represented by an pendulum model with an specific and fixed configuration.

50 Many improvements and new models have been developed to solve some inaccuracies or to
51 represent special behaviors [9][10][11][12]. This work presents one of those improvements for dealing
52 with the robot inaccuracies such as material flexibility or component tolerances that are very difficult
53 to be modeled. Experimentally-based, system errors have been quantified and used to improve the
54 inverted pendulum model, as will be described in following sections. By means of an error scheduling
55 method, the model parameters for control can be dynamically computed. The experimental platform
56 used in this work is the humanoid robot TEO (*Task Environment Operator*) from University Carlos III of
57 Madrid [13], shown in Fig.1.

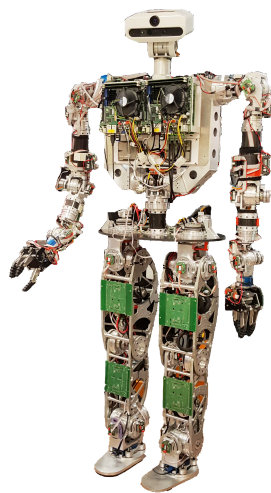


Figure 1. TEO Humanoid Robot from University Carlos III of Madrid

58 2. BACKGROUND

59 To solve complexity, the humanoid robot is usually represented by means of simplified models
60 that enable an easy way of designing controllers. These models represents kinematics and dynamics
61 of the robotic system in action. Taking in account different parameters of the robot, such as the mass,
62 the location of its CoM, inertia tensors, etc. many approximate models of the robot for each task
63 context can be established. This work is focused in the study of simplified models applied in balance
64 control and how inherent model errors can be overcome to improve robot operation. This background

65 is mainly divided in the enumeration of some simplified models and how they are used in balance
 66 control.

67 *2.1. Robot Simplified models*

68 The simplest model for representing robot's kinematics and dynamics is the two dimensional
 69 inverted pendulum with one or two DoF [14]. These models represent a concentrated CoM linked
 70 rigidly to the ground by one rotational joint like in Fig.2 left, or including a linear joint like in Fig.2
 71 right.

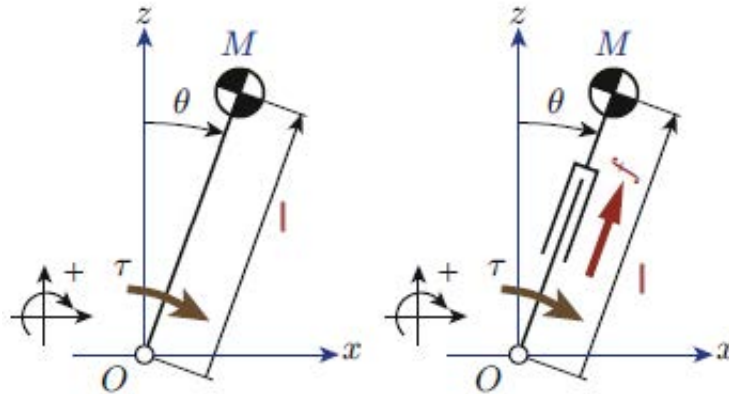


Figure 2. Basic Inverted Pendulum Models in x-z plane. 1DoF (left) and 2DoF (right)

72 In the case of Fig.2 left, the movement of the CoM is defined by the following equation:

$$\tau = -ml^2\ddot{\theta} + mgl \sin \theta \quad (1)$$

73 where m is the mass of the CoM, l the pendulum longitude, τ the torque at the pivot point and
 74 θ is the pendulum angle. But this is a non-linear equation that makes its implementation in a robot
 75 controller more difficult. To overcome this problem it is assumed that θ is small enough to consider
 76 $\sin \theta = \theta$. Then, the resulting model is one of the most famous models used in humanoid robotics. It is
 77 the Three Dimensional Linear Inverted Pendulum (3DLIPM) shown in Fig.3 and proposed by Kajita
 78 [15].

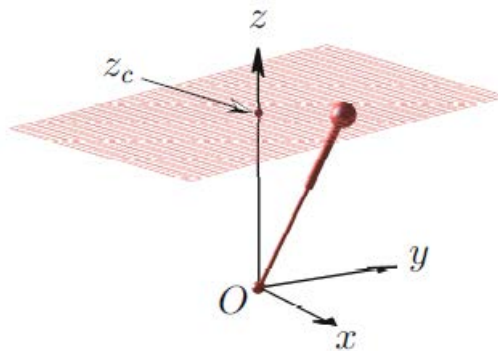


Figure 3. 3DLIPM Model [14]

79 Then, equation (1) becomes (for 2D case in plane x-z):

$$\tau = -ml^2\ddot{\theta} + mgl\theta \quad (2)$$

80 with the z -coordinate movement constrained to an horizontal plane,

$$z = z_c \quad (3)$$

81 The main advantage of 3DLIPM is the linear equations that are very easy to program in a computer.
82 They are mainly used for walking pattern generation and balance control. The application of this
83 equation for balance control is possible whether ground reaction (vertical force) and torques in the
84 robot's ankle joint, which correspond with the point O of the model, can be measured. It has been
85 achieved by the use of Force/Torque (F/T) sensors at foot level, such as JR3 sensors assembled in robot
86 TEO feet (Fig.4).

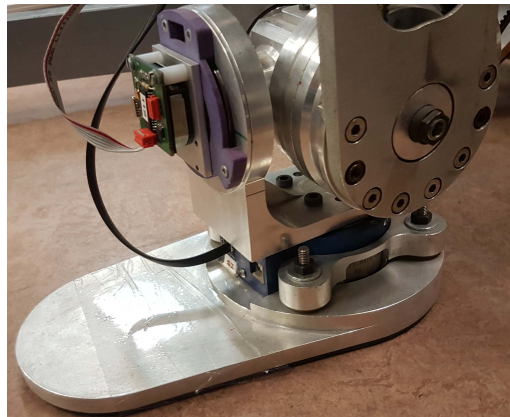


Figure 4. TEO's ankle joints with JR3 F/T sensor

87 But 3DLIPM doesn't provide information about body accelerations and inertias, that are very
88 useful information for a biped robot during a dynamic walking task. This issue was solved with the
89 development of the *cart-table* simplified model (Fig. 5). In this case, the information need by the model
90 is provided by Inertial Measurement Units (IMUs) which sense velocities and accelerations of the robot
91 body.

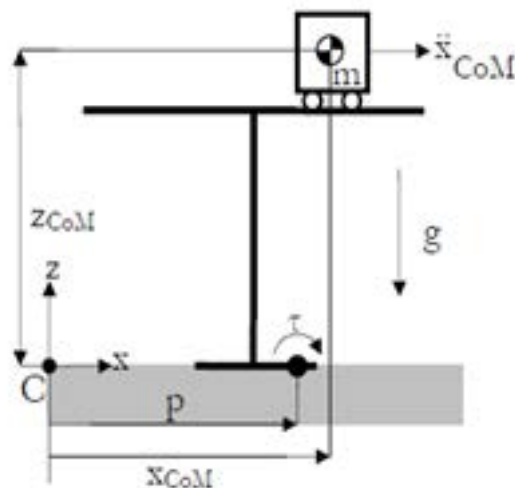


Figure 5. Cart-table simplified model

92 Cart-table and 3DLIPM are the most used simplified models in balance control. Nevertheless,
93 other researchers lead their works towards multi-link models, where they use a precise knowledge
94 about dynamics of each robot link [16][17].

95 2.2. Zero Moment Point and balance

96 The study of humanoid robots balance has been supported by the simplified models described
 97 before. Many tools have been developed to describe the kinematic and dynamic behavior of a
 98 humanoid when it performs tasks. Taking in account that one of the main goals of a humanoid robot is
 99 to achieve stable walking behaviors, these tools have been widely studied in this field.

100 The development of a humanoid balance control architecture is mainly related to the study of
 101 two specific reference points. The first one is the Center of Mass used to model humanoid body as
 102 described in the previous subsection. But CoM doesn't provide useful information about the body
 103 balance status. Zero Moment Point (ZMP) introduced by Vukobratovic in [18] is the first and the main
 104 tool developed for describing body's static equilibrium. The ZMP is a point in the robot support base,
 105 usually the ground, where the resulting torque caused by any kind of force acting over the robot's
 106 body is equal to zero. Fig. 6 illustrates the ZMP location P and Eq. (6) defines it mathematically.

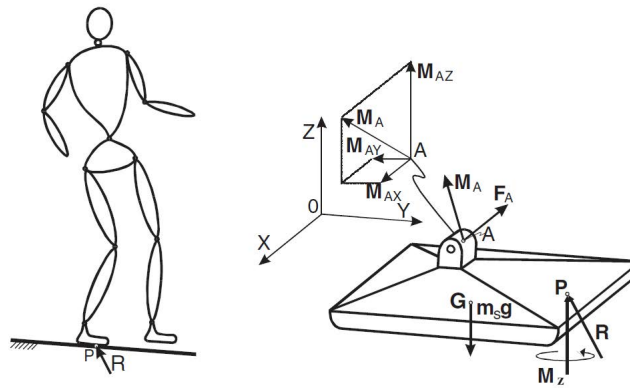


Figure 6. ZMP

$$P_x = -\frac{\sum x \cdot F_z}{\sum F_z} \quad (4)$$

107 In Eq. (6), for the coordinate x , the sum of the torques produced by the mass of each link of the
 108 body due to gravity is divided by the sum of reaction forces. If the value of ZMP coordinate lays inside
 109 the support polygon of the robot, the balance of the robot can be guaranteed. But when the ZMP is in
 110 the edge of the support area, the humanoid body can loose balance and fall down.

111 The computation of the ZMP depends on the posture of the robot and the location of the CoM
 112 of each limb. Due to that, ZMP calculation gains the advantage of representing the robot body as a
 113 simplified model for two main reason. The first one is the simplicity of the equations used for ZMP
 114 computation. The second reason is the possibility of using F/T sensors to measure all the forces and
 115 torques need for ZMP computation. The model applied in this work is the 3DLIPM modified to match
 116 with the TEO robot structure, as can be observed in Fig. 7.

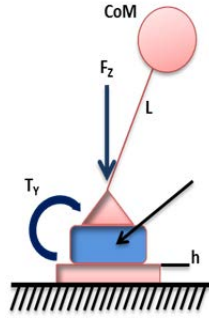


Figure 7. LIPM with F/T sensor

117 When a biped robot is supporting its body on one foot, the robot ankle is considered the pivot
 118 point connected to the robot's CoM by means of a massless leg. The simplest model only considers
 119 the gravitational force exerted to the mechanism and the pendulum motion is represented by Eq. (2).
 120 According to [19], the ZMP equation in the sagittal plane obtained from the LIPM when the robot is
 121 standing on one foot:

$$x_{ZMP} = -\frac{\tau_y + hF_x}{mg} \quad (5)$$

122 where τ_y is the torque at the pivot point around y axis, F_x is the measured force in the x direction
 123 and h is the distance from the ground to the location of the sensor (generally the sole height). But when
 124 the robot stands in double support -both feet lie on the ground-, ZMP obtained from each foot is used
 125 to compute the global ZMP [14]:

$$x_{ZMP_{DS}} = -\frac{x_{ZMP}^R \cdot F_z^R + x_{ZMP}^L \cdot F_z^L}{F_z^R + F_z^L} \quad (6)$$

126 where upper index R represents the right foot and L the left one. Even when the robot is in double
 127 support-phase and two pivot points at the ankle joints exist, the inverted pendulum can be used. If
 128 the movement is in the sagittal plane, the robot behaves as a single inverted pendulum because both
 129 ankles have the same movement along the x axis.

130 2.3. Balance control

131 One of the main skills defining the human being is the capacity of walking upright. In the same
 132 manner, this is one of the main features that a humanoid robot must to achieve. The key question
 133 relays on the balance of the upright posture to avoid falls, during a walking task or standing still. The
 134 use of the simplified models of the body and tools such as ZMP enables the deployment of stabilizers
 135 to maintain equilibrium.

136 Before performing a walking task, the humanoid robot must to keep an upright stable posture.
 137 In this situation, the robot must deal with unexpected disturbances as the first premise to develop
 138 a balance control architecture. So, achieving this upright stable posture is the first stage to develop
 139 an stabilizer. One of the main techniques to start the development of a balance control architecture
 140 is based on push-recovery experiments, like shown in Fig. 8. The robot must deal with unexpected
 141 disturbances represented as forces applied to it. If unexpected disturbances appear and depending
 142 on the intensity level of the disturbance, different control strategies can be set [20]: ankle, hip and
 143 step strategy. For low intensity disturbances, the body can be considered as a nearly single stiff
 144 pendulum, where balance adjustments are mainly made in the ankle joints of the robot [12]. The hip
 145 strategy is applied when the external disturbance increases and the ankle strategy is not enough to
 146 keep balance. When acting this strategy, the robot can move its hip independently or in combination
 147 with the ankle strategy. Then, the robot model has to be modified, considering a double inverted

148 pendulum [20][21]. The double inverted pendulum consists of an upper link and a lower link, which
 149 involves that each single pendulum has an influence on the other one. Step strategy is only used when
 150 postural corrections become insufficient and the base of support must be adjusted. Taking this in
 151 account, the very beginning phase to develop a stabilizer is to deploy the control system for each
 152 strategy, starting from the ankle one.

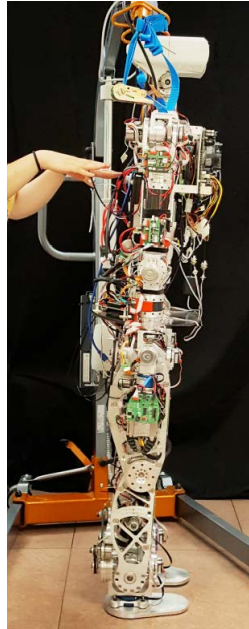


Figure 8. Push-recovery experiment with TEO robot

153 Balance control with the ankle strategy concept is applicable both to standing in upright posture
 154 and, as well, to walking tasks. In both situations, the robot is modeled as an inverted pendulum. The
 155 disturbance is a force applied to the CoM of the model. This force can lead the ZMP to be out of the
 156 support polygon and the robot would lose balance. Then, the robot must counteract this disturbance
 157 applying a torque in the ankle joints, trying to maintain ZMP inside the support area. This kind of
 158 control is called *ZMP control by ankle torque* [22][23] and it is represented by the control architecture
 159 depicted in Fig. 9.

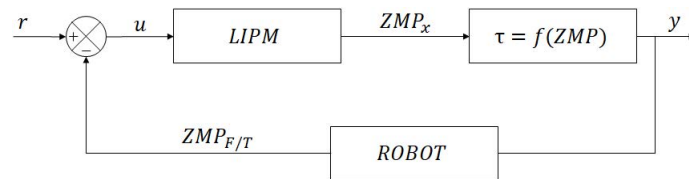


Figure 9. Basic ZMP position controller

160 **The balance control architecture presented PID controller?? (ver KAYNOV) Model**
 161 **Controller??**

162 But traditional PID Control relies on the proper the proper selection of values to be used for the
 163 Proportional (P), Integral (I), and Derivative (D) constants for a linearized working point [24]. If the
 164 process is non linear, the control designer must then continuously evaluate it and tune the constants.
 165 Instead using PID controllers, Model-Based Controllers are able to learn how a process responds to
 166 changes, and in turn, they can automatically make the tuning adjustments that would traditionally be
 167 manual.

168 **3. PROBLEM STATEMENT**

169 However, there are many errors that the balance control system must deal with. Simplified model
 170 control approaches always introduce errors. Pendulum mathematical model is not linear, but ZMP
 171 equations are obtained from a linear pendulum. When the angle of the pendulum is small enough, it is
 172 assumed that $\sin \theta = \theta$, which introduces an error to the system. The mass of the Center of Gravity
 173 (CoG) is also an approximated value of the whole robot mass, even its location can change. Joining all
 174 this assumptions, errors in the system become remarkable.

175 Also, there can be measurement deviations in the Force-Torque (F/T) sensors due to calibration
 176 errors, or in analogue to digital data conversions. Other systematic errors as the flexibility of the
 177 structure (due to the height of the robot), loosenesses between mechanical parts (as transmissions or
 178 unions of pieces), and small irregularities in the ground are usually not considered. All of these errors
 179 lead to increase the control effort and makes the control tuning task more difficult.

180 The aim of this work is to improve the ZMP control system described before, proposing an
 181 Adjusted LIPM (ALIPM). This model will include the errors depicted in Fig.10 and more. The
 182 procedure to model this error is based on push-recovery experiments in which the ZMP is computed
 183 thanks to the measures provided by F/T sensors. Then, the real ZMP is compared with the planned
 184 ZMP, obtaining the error. Finally, the error is introduced in the model as a fictitious force that modifies
 185 the inverted pendulum model behavior.

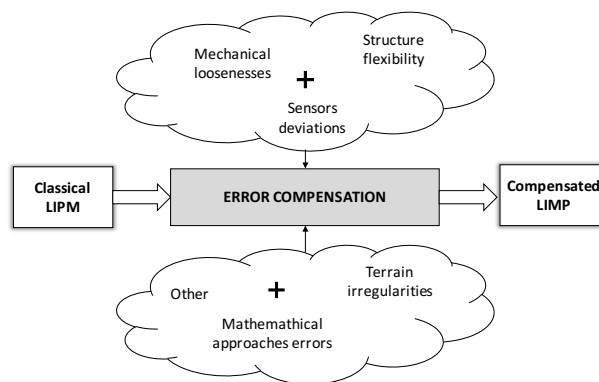


Figure 10. Error compensation diagram

186 From the control point of view, the real humanoid mechanism is slightly flexible [22]. Usually the
 187 flexibility is close related to the robot height and, although robot designers try make stiff structures, it is
 188 impossible to eliminate it. Because of this compliance, the humanoid robot exhibits the characteristics
 189 of a lightly damped structure. For example, in a static case when the ankle joint is under position
 190 control, a pushing external force can easily excite an oscillation. This oscillation exists even when the
 191 position error in every joint is zero. As well, there are other error sources that have influence in the
 192 correlation of the robot with model (Fig.10). But it is very difficult to identify and define these errors
 193 mathematically.

194 The existence of those error have high influence on the ZMP computation and, for that, on the
 195 balance control system. Fig. 11 illustrates how robotic system inaccuracies and other error sources
 196 affects to the location of the ZMP. In this example, u denotes the model angle expected caused by
 197 the commanded joint torque. The expected ZMP would be represented by x_{exp} . If we consider only
 198 the error introduced by the robot flexibility, the ZMP location would be the one represented by x_{err} .
 199 Nevertheless, the real ZMP computed using the forces and torques measured is $x_{F/T}$

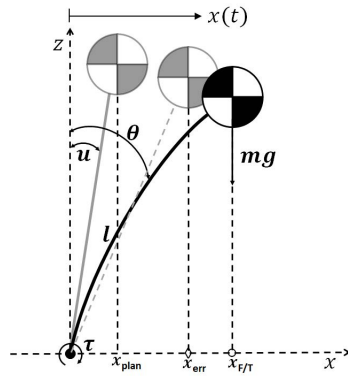


Figure 11. Single inverted pendulum model [22]

200 Then, the problem is the mismatch between the ZMP expected or planned and the real ZMP
 201 measured with the F/T sensors. In order to reduce this gap, this work propose a model improvement
 202 closer to the real robot behavior. Furthermore, ZMP control architecture for keeping balance can be as
 203 well improved.

204 4. METHODS AND EXPERIMENTAL PROCEDURE

205 To achieve it, the error has been modeled using the information of the F/T sensors installed
 206 in the ankles of the robot. All the effects caused by any disturbance are reflected in the forces and
 207 torques measured by the sensors. In this way, it is necessary to separate the information related to the
 208 inaccuracies and the other related to the expected behavior. Some assumptions need to be made before
 209 performing this procedure. The first one is the necessity of establishing the inverted pendulum model
 210 parameters: CoM location and mass. They come from the robot design but they are not complete
 211 accurate because differences between CAD designs and real implementation. The correction of this
 212 parameters using the real robot is not possible, so it is assumed the use of the theoretical values.
 213 The second assumption is related to the planning of balance control task. Taking into account the
 214 established model, ZMP location can be planned. That is, ZMP location can be pre-planned to remain
 215 always inside the support polygon. It is desirable that balance plan will be close to reality in order to
 216 reduce the effort of the control system. This means that lower gains will be need to adjust the control
 217 system.

218 The method used to develop the new improved model is the following. Based on open-loop
 219 system push-recovery set of experiments, the measurements of the F/T sensors are captured and
 220 processed. Then, with this information, ZMP real $x_{F/T}$ is computed and compared with ZMP expected
 221 x_{exp} . The difference between them is modeled and one equation describing this error is obtained. The
 222 modeled error is included in the original model as a fictitious force that corrects the difference found.
 223 Once the new model has been obtained, the new planned ZMP behavior is close to the ZMP measured.

224 4.1. Study of the system response

225 To introduce into TEO simplified model all the errors mentioned before, the procedure
 226 summarized in Fig. 12 has been followed.

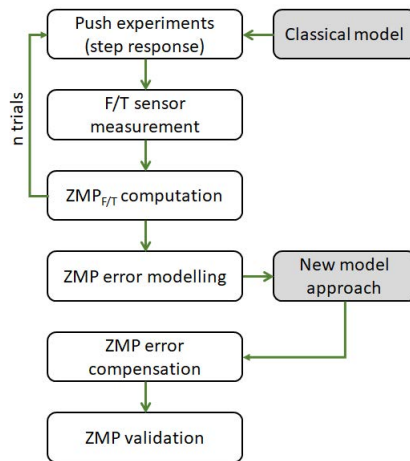


Figure 12. Experimental procedure diagram

227 The first stage is to fix the inverted pendulum parameters with the characteristics of the humanoid
 228 robot TEO. The robot weight is 62.6kg and the longitude from the ground to the CoM is 0.8927m (the
 229 pendulum length). Then, the expected movement of the robot actuated by a pushing force has been
 230 experimented. This behavior is similar to the study of the response of a system with an step
 231 input. To illustrate the method only the results from the saggital plane (x-z) of the robot is presented
 232 because the experimental methodology for the frontal plane (y-z) is the same and similar results has
 233 been obtained. In this way, the experimental setup is represented by Fig. 13. The robot is in a flat
 234 ground environment with both feet on the ground (double support). Therefore, the support area
 235 includes the robot footprints and the common tangents between them.

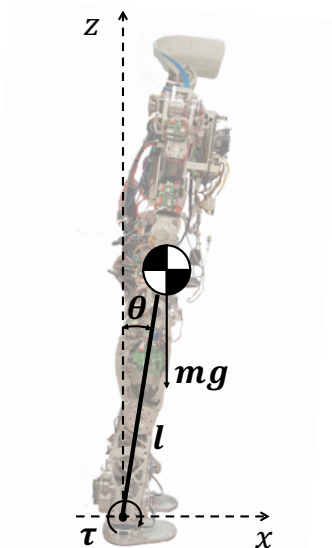


Figure 13. Experimental setup of TEO robot

236 After performing a set of trials, the results are shown in Fig. 14. This figure represents the ZMP
 237 measured (the oscillating signals) and the expected ZMP (the step form signals). Each pair of ZMP
 238 signal (oscillating-step) correspond to a specific push force applied to the robot. If we examine each
 239 pair, some conclusions can be extracted. Bigger disturbances imply further location of the ZMP from
 240 its origin, making the robot more unstable because ZMP is closer to the support polygon edge. It
 241 means that the model angle is bigger and the errors have more influence, mainly robot flexibility and

242 mechanical tolerances. For this reason, the steady state error is as well higher. Furthermore, the system
 243 have a higher initial oscillating response, which is not desirable when ZMP is located near the edge of
 244 the support polygon.

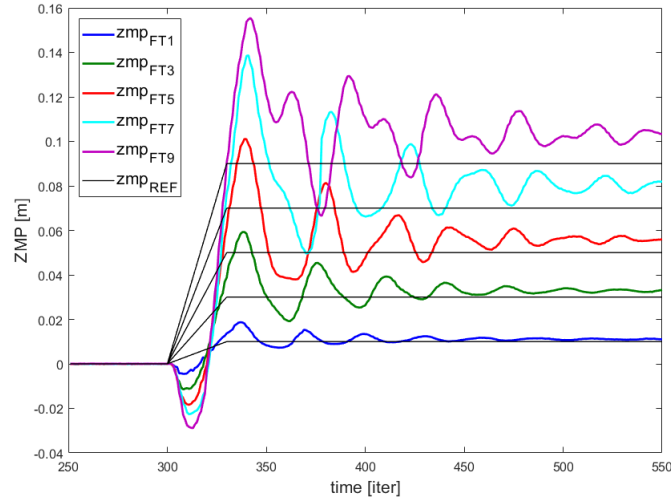


Figure 14. Step response experiments

245 This dataset is the base for developing an improved ZMP control without the necessity of low
 246 level position or torque controller parameters tuning. The objective of next steps is to obtain a transfer
 247 function modeling the ZMP behavior. The resulting transfer function, that models ZMP deviations,
 248 will be added to the classic LIPM with two main responsibilities: the elimination of steady state error
 249 and the reduction of transient oscillation and overshooting.

250 4.2. Adjusted linear inverted pendulum model

251 To accomplish the ZMP control requirements, this work proposes an improvement model derived
 252 from the classic LIPM. The objective is to modify the initial model adding a system that represents the
 253 errors of the real robot obtained from experimentation. Then, balance parameters measured will have
 254 less deviation from planned and the control parameters can be reduced. Fig. 15 represents the complete
 255 model in which a spring k_a and a damper B_a have been added to the initial inverted pendulum model.
 256 These mechanical model try to compensate the steady state response (k_a) and the transient response to
 257 limit oscillations (B_a).

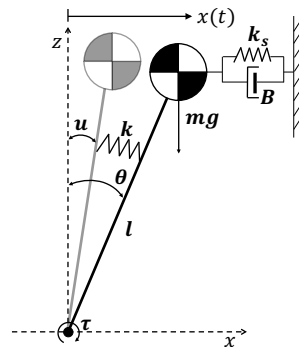


Figure 15. Proposed compensated inverted pendulum model

258 Then, the equation of motion of the model shown in Fig. 15 is given by:

$$\tau = -ml \frac{d^2}{dt^2}x(t) - B_a l \frac{d}{dt}x(t) - k_a l x(t) + mgx(t) \quad (7)$$

259 where $x(t)$ is the CoM movement, m is the pendulum mass located at the CoM, l its longitude,
 260 k_a the spring constant and B_a the damper constant. The displacement of the CoM is small enough to
 261 assume $\sin\theta = \theta$. Then, equation (7) becomes:

$$\tau = -ml^2\ddot{\theta}(t) - B_a l\dot{\theta}(t) - k_a l\theta(t) + mgl\theta(t) \quad (8)$$

262 Torque can be also obtained from the ZMP measurement as:

$$\tau_y = -x_{FT} \cdot mg \quad (9)$$

263 where x_{FT} is the measured ZMP from the sensors. Combining both equations we obtain:

$$-ml^2\ddot{\theta}(t) - B_a l\dot{\theta}(t) - k_a l\theta(t) + mgl\theta(t) = -x_{FT}(t)mg \quad (10)$$

264 Finally, the transfer function obtained from equation (10) is:

$$\frac{\Theta(S)}{X(S)} = \frac{K}{S^2 + \alpha S + \beta} \quad (11)$$

265 where $K = g/l^2$, $\alpha = B_a/ml$, and $\beta = (K_a - g)/l$. In the steady state, when time goes to infinity,
 266 the DC gain of the system is represented by Eq. (12), that only depends on the K_a parameter. This one
 267 is in charge of eliminate the static error.

$$K_s = \frac{K}{\beta} \quad (12)$$

268 4.3. Steady state ZMP error characterization

269 The next step is to characterize the deviation of the ZMP. Even though ankle position control
 270 succeed the ZMP measurement presents deviations. From trials dataset depicted in Fig. 14, the deviation
 271 of the ZMP can be determined. Fig. 16 represents the deviation of the $ZMP_{F/T}$ from the ZMP_{exp} .

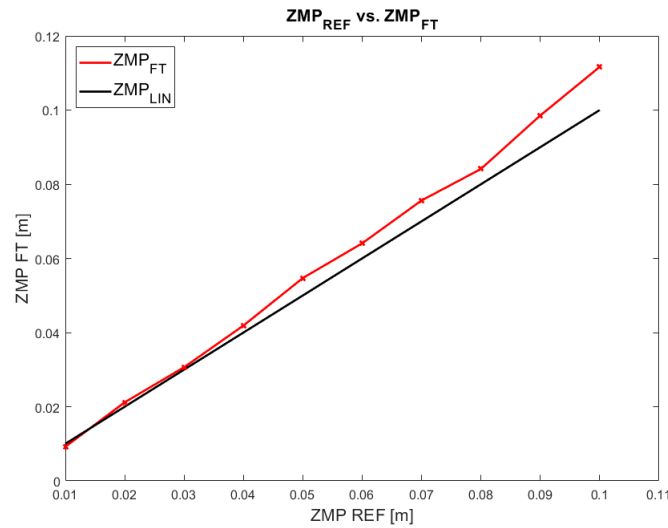


Figure 16. Experimental $ZMP_{exp} - ZMP_{F/T}$ deviation

272 The deviation in each test point is used to fit it to a second order polynomial equation (13). This
 273 equation represents the real ZMP $x_{F/T}$ measured by the ankle sensors:

$$x_{F/T} = a \cdot x_{exp}^2 + b \cdot x_{exp} + c \quad (13)$$

274 where $a = 0.834$, $b = 1.024$ and $c = -0.0004$.

275 This equation represents the steady state error of the open-loop system for each working point.
 276 Equation (13) and Equation (12) are the base for planing the evolution of the joint angle and, therefore,
 277 ZMP location. Once the static error has been minimized the transient response is optimized to reduce
 278 the level of oscillations.

279 4.4. ZMP transient response characterization

280 Linear inverted pendulum is inherently unstable. It is necessary to develop a controller to stabilize
 281 it against any kind of disturbance. Meanwhile the step response of the inverted pendulum goes to
 282 infinite, higher order systems have stable behaviors. Fig.17 shows the comparison of the LIPM vs.
 283 ALIPM transfer functions response to a simulated step input. This behavior also means that the
 284 dynamic parameters can be adjusted to higher values in the ALIPM case, having more margin to be
 285 configured.

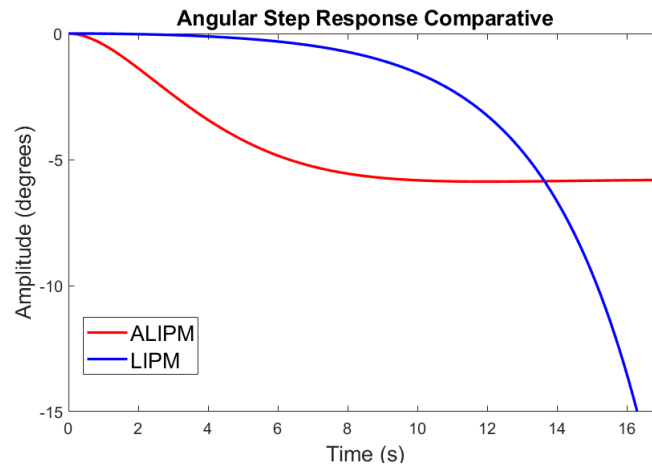


Figure 17. Angular step response LIPM-ALIPM

286 The behavior of the humanoid robot system has been demonstrated as a under damped system.
 287 Selecting appropriate gain and dynamic parameters it is possible manipulate the overall response of
 288 the system, reducing the over shooting and oscillation of the system. ZMP oscillations have higher
 289 values when its location is further from the origin and, as well, when the input angle have a high
 290 variation. This relation between ZMP and ankle angle allows the reduction of the oscillation level by
 291 means of angle planning. In (11), dynamic parameters can be configured, for example, to limit the over
 292 shooting level. Figure 18 shows the signal obtained from the simulation of a disturbance causing a
 293 ZMP variation of 9cm. The dynamic parameters were designed to obtain an over damped response
 294 ($\zeta = 0.8$, $\omega_n = 0.4376$)

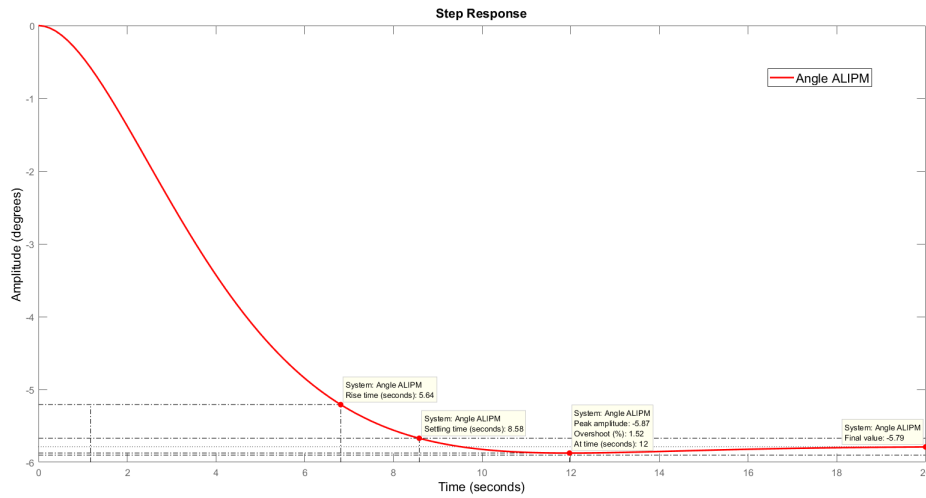


Figure 18. Step response ALIPM

295 Then, selecting the proper parameters it is possible to modulate the dynamics of the robot and
 296 reduce undesired oscillation levels on the robot.

297 4.5. ZMP control

298 Classical control architectures, such as the one shown in Fig.9, are based the linearisation of
 299 the controller around a working point. It means that the controller is has almost no error in this
 300 working point and it has more error as the control target is further than this point. In this work, a
 301 non-linear solution is proposed, based on the *Gain Scheduled Matching*. The main goal is to select
 302 dynamically the most appropriate parameters for each working point of the controller. In control
 303 theory, a gain-scheduled controller is a system control architecture in which its gains are automatically
 304 adjusted as a function of time, operating condition, or plant parameters [16]. Gain scheduling is a
 305 common strategy for controlling systems in which its dynamics change with such variables. Typically,
 306 gain-scheduled controllers are fixed single loop or multiloop control structures that use lookup tables
 307 to specify gain values as a function of the scheduling variables. For tuning purposes, it is convenient to
 308 replace lookup tables with parametric gain surfaces, such as fuzzy surfaces [25][26]. A parametric gain
 309 surface is a basis function expansion in which its coefficients are tunable. For applications where gains
 310 vary smoothly with the scheduling variables, this approach lets tune a few coefficients rather than
 311 many individual lookup-table entries, drastically reducing the number of parameters. This approach
 312 also provides explicit formulas for the gains, and ensures smooth transitions between operating points.

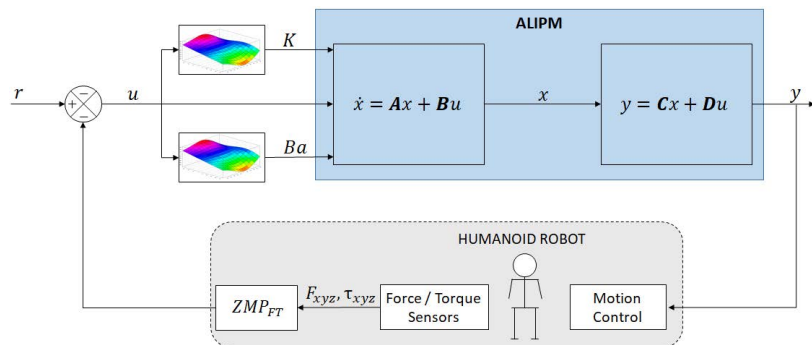


Figure 19. TEO ZMP controller

313 The control architecture is presented in Fig.19, similar to the human-inspired control architecture
 314 presented in [27]. In this case, there is a preprocessing module for control parameters planning.
 315 Depending on the input u the appropriate values for K and B_a can be selected. Then, these parameters
 316 are used for computing the values of the coefficients of the ALIMP' state space model. Finally, the
 317 ALIMP module outputs the ankle angle to be commanded to the robot.

318 4.6. Experimental validation

319 To check the feasibility of the proposed system, it was tested experimentally performing a set
 320 of trials for capturing the response of the control system against a variation on the ZMP target. The
 321 ALIMP state space model was customized with the parameters for each ZMP target, following the
 322 step pattern. Then, the output of the model was the customized angle commands following the
 323 ZMP planning. Table 1 shows numeric result of ZMP location, comparing the values obtained from
 324 the classical approach and the ALIMP approach. It can be observed that the static error is reduced
 325 in each working point. Even in the most critical ZMP location ($ZMP = 10cm$), the error has been
 326 reduced in more than 80% between the obtained ZMP measurements using the classical LIPM and the
 327 compensated model proposed in this paper.

Table 1. ZMP comparison using Classical and Proposed LIMP

ZMP_{REF} [m]	ZMP_{FT} [m]			
	Classical model	% error	Proposed model	% error
0.00	$5 \cdot 10^{-5}$	0.0	$2 \cdot 10^{-7}$	0.0
0.01	0.0092	8.2	0.0100	0.0
0.02	0.0211	6.0	0.0201	0.5
0.03	0.0306	2.2	0.0310	3.3
0.04	0.0419	4.8	0.0412	3.0
0.05	0.0547	9.4	0.0512	2.4
0.06	0.0641	6.8	0.0620	3.3
0.07	0.0756	8.0	0.0714	2.0
0.08	0.0841	5.2	0.0816	2.0
0.09	0.0902	9.5	0.0989	0.2
0.10	0.1116	11.6	0.1020	2.0

328 Data from Table 1 has been depicted in Fig.20. It can be observed that the error in the
 329 classical system is higher when the ZMP location is further from the initial zero position (blue
 330 line). Furthermore, the ALIMP curve is more adjusted to the desired linear response (red line).

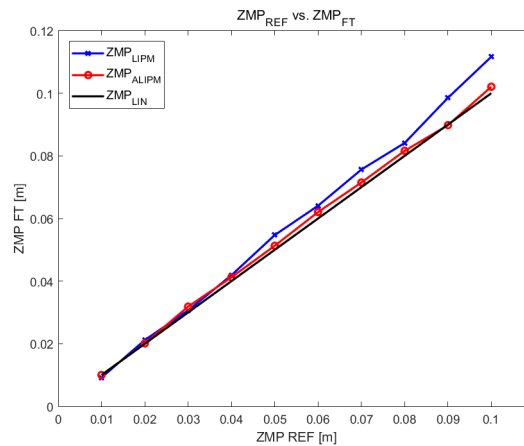


Figure 20. ZMP comparison using Classical and Proposed LIMP

331 About the dynamic response of the system, 21 depicts the results from all the trials performed.
332 Comparing this figure with Fig.14, it is easy to observe that the level and the duration of oscillations
333 has been reduced. Although, the over shooting has similar levels in some experiments, the state of the
334 robot is stabilized in general earlier than the classical architecture.

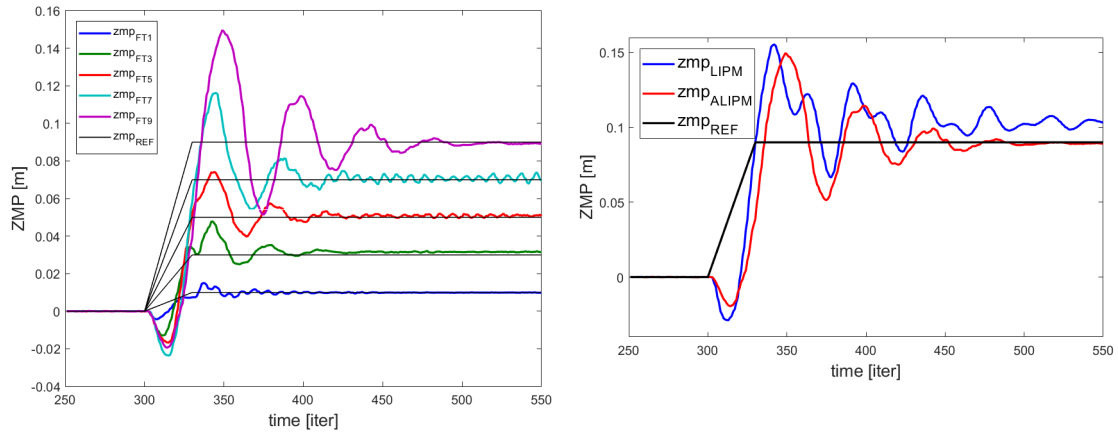


Figure 21. ZMP step responses comparative.

335 5. CONCLUSIONS AND FUTURE WORKS

336 Humanoid balance control is based on the knowledge of certain equilibrium indicators. These
337 parameters are materialized in mathematical models that represent simplifications of the humanoid
338 body behavior. The less simplified is the model, the more accurate is the control performance but then
339 computational complexity is higher. Classical simplified models, such as the LIPM, have a high level
340 of simplification. It can model the walking behavior and balance but, as well, introduce approximation
341 errors. On the other hand, the robot mechanics and electronics have inherent inaccuracies that are
342 added to those from the model. This work has presented one method to modify the humanoid robot
343 model to reduce these inaccuracies and to improve the balance control system. The experimental
344 procedure, founded in push-recovery trials, has been used to determine the steady state error and
345 the dynamic response of the system. This procedure can be applied to any kind of humanoid robot
346 because is independent of the system and it is able to characterize any kind of inaccuracy.

347 The resulting model, name here as ALIPM, is the base to implement a model-based balance
348 controller. Linear balance controllers based on the use of these simplified models need a very precise
349 and complex tuning to find the optimal control parameters. Furthermore, these kind of controllers
350 are designed to operate around a working point with a minimum error. Nevertheless, the balance
351 architecture proposed, using the ALIPM, has been conceived to operate in multiple working points,
352 minimizing the error in each one. The ALIPM is a template that must be fulfilled with the proper
353 parameters for each specific working point, which is related to the balance status of the robot (ZMP).
354 These parameters define two things: the evolution of the ZMP between two consecutive postures and
355 the level of error in each ZMP. In the first case, it has been achieved a smoother trajectory between
356 postures reducing undesired oscillations, especially in critical ZMP locations. In the second case, the
357 error between desired ZMP location and the measured ZMP has been reduced. These results are
358 shown in Table 1.

359 Currently, the described work deals with the humanoid robot modeling in a laboratory
360 environment with flat surfaces. The next step is to extend the procedure to models applied to other
361 robot behaviors, such as walking in uneven surfaces. Moreover, new improvements are need to
362 evaluate the influence of the upper body movement or the behavior of the control system when
363 carrying objects.

364 ACKNOWLEDGMENT

365 The research leading to these results has received funding from the RoboCity2030-III-CM project
366 (Robótica aplicada a la mejora de la calidad de vida de los ciudadanos. fase III; S2013/MIT-2748),
367 funded by Programas de Actividades I+D en la Comunidad de Madrid and cofunded by Structural
368 Funds of the EU. We would like to thank Maria Dolores Pinel and Aitor Gonzalez for their collaboration
369 during the experimental and data processing phases.

370 References

- 371 1. Henze, B.; Dietrich, A.; Ott, C. An approach to combine balancing with hierarchical whole-body control
372 for legged humanoid robots. *IEEE Robotics and Automation Letters* **2016**, *1*, 700–707.
- 373 2. Morisawa, M.; Kita, N.; Nakaoka, S.; Kaneko, K.; Kajita, S.; Kanehiro, F. Biped locomotion control for
374 uneven terrain with narrow support region. *System Integration (SII), 2014 IEEE/SICE International Symposium*
375 *on 2014*, pp. 34–39.
- 376 3. Budiharto, W.; Moniaga, J.; Aulia, M.; Aulia, A. A framework for obstacles avoidance of humanoid robot
377 using stereo vision. *International Journal of Advanced Robotic Systems* **2013**, *10*, 204.
- 378 4. McGill, S.G.; Zhang, Y.; Vadakedathu, L.; Sreekumar, A.; Yi, S.J.; Lee, D.D. Comparison of Obstacle
379 Avoidance Behaviors for a Humanoid Robot in Real and Simulated Environments. *Humanoid Robots, 2012.*
380 *IEEE International Conference on 2012*.
- 381 5. Arbulu, M.; Balaguer, C. Real-time gait planning for the humanoid robot Rh-1 using the local axis gait
382 algorithm. *International Journal of Humanoid Robotics* **2009**, *6*.

- 383 6. Stephens, B. Humanoid push recovery. *Humanoid Robots, 2007 7th IEEE-RAS International Conference on*
384 *2007*, pp. 589–595.
- 385 7. Yun, S.k.; Goswami, A.; Sakagami, Y. Safe fall: Humanoid robot fall direction change through intelligent
386 stepping and inertia shaping. *2009 IEEE International Conference on Robotics and Automation 2009*, pp.
387 781–787.
- 388 8. Agravante, D.J.; Sherikov, A.; Wieber, P.B.; Cherubini, A.; Kheddar, A. Walking pattern generators designed
389 for physical collaboration. *Robotics and Automation (ICRA), 2016 IEEE International Conference on 2016*, pp.
390 1573–1578.
- 391 9. Yin, C. Walking Stability of a Humanoid Robot Based on Fictitious Zero-Moment Point. *Power Engineering*
392 *2006*, pp. 1–6.
- 393 10. Feng, S.; Sun, Z. Biped Robot Walking Using Three-Mass Linear **2008**. pp. 371–380.
- 394 11. Lee, S.H.; Goswami, A. The reaction mass pendulum (RMP) model for humanoid robot gait and balance
395 control. In *Humanoid Robots*, First ed.; Choi, B., Ed.; InTech, 2009; Vol. 71, pp. 169–186.
- 396 12. González-Fierro, M.; Monje, C.; Balaguer, C. Fractional Control of a Humanoid Robot Reduced Model
397 with Model Disturbances. *Cybernetics and Systems 2016*, 47.
- 398 13. Martínez, S.; Monje, C.A.; Jardón, A.; Pierro, P.; Balaguer, C.; Muñoz, D. TEO: FULL-SIZE HUMANOID
399 ROBOT DESIGN POWERED BY A FUEL CELL SYSTEM. *Cybernetics and Systems 2012*, 43, 163–180.
- 400 14. Kajita, S.; Hirukawa, H.; Harada, K.; Yokoi, K. Introduction to Humanoid Robotics. In *Springer Tracts in*
401 *Advanced Robotics*; Siciliano, B.; Khatib, O., Eds.; Springer-Verlag Berlin Heidelberg: Berlin, Heidelberg,
402 2014; Vol. 101.
- 403 15. Kajita, S.; Kanehiro, F.; Kaneko, K.; Yokoi, K.; Hirukawa, H. The 3D linear inverted pendulum mode:
404 a simple modeling for a biped walking pattern generation. *Proceedings 2001 IEEE/RSJ International*
405 *Conference on Intelligent Robots and Systems; IEEE: Maui, 2001; Vol. 1, pp. 239–246.*
- 406 16. Kljuno, E.; Williams, R.L. Humanoid Walking Robot: Modeling, Inverse Dynamics, and Gain Scheduling
407 Control. *Journal of Robotics 2010*, 2010.
- 408 17. Feng, S.; Sun, Z. Biped robot walking using three-mass linear inverted pendulum model. In *In International*
409 *Conference on Intelligent Robotics and Applications; Xiong, C.; Huang, Y., Eds.; Springer Berlin Heidelberg:*
410 *Berlin, Heidelberg, 2008; pp. 371–380.*
- 411 18. Vukobratovic, M.; Borovac, B. Zero-moment point — thirty five years of its life. *International Journal of*
412 *Humanoid Robotics 2004*, 1, 157–173.
- 413 19. Kajita, S.; Kanehiro, F.; Kaneko, K.; Fujiwara, K.; Harada, K.; Yokoi, K.; Hirukawa, H. Biped walking pattern
414 generation by using preview control of zero-moment point. *Proceedings of the 2003 IEEE International*
415 *Conference on Robotics and Automation; IEEE: Taipei, Taiwan, 2003; pp. 1620–1626.*
- 416 20. Nenchev, D.N.; Nishio, A. Ankle and hip strategies for balance recovery of a biped subjected to an impact.
417 *Robotica 2008*, 26, 643–653.
- 418 21. Kajita, S.; Yokoi, K.; Saigo, M.; Tanie, K. Balancing a humanoid robot using backdrive concerned torque
419 control and direct angular momentum feedback. *Robotics and Automation, 2001. Proceedings 2001 ICRA.*
420 *IEEE International Conference on 2001*, 4, 3376–3382.
- 421 22. Kim, J.H.; Oh, J.H. Walking control of the humanoid platform KHR-1 based on torque feedback control.
422 *IEEE International Conference on Robotics and Automation, 2004. Proceedings. ICRA '04. 2004 2004*, 1, 623–628.
- 423 23. Kaynov, D. Open motion control architecture for humanoid robots. PhD thesis, University Carlos III of
424 Madrid, 2009.
- 425 24. Ogata, K.; Yang, Y. Modern control engineering; Prentice-Hall Englewood Cliffs, NJ: Upper Saddle River,
426 New Jersey, 1970.
- 427 25. Safiotti, A. Fuzzy logic in autonomous robotics: behavior coordination. *Proceedings of 6th International*
428 *Fuzzy Systems Conference 1997*, 1, 573–578.
- 429 26. Takagi, T.; Sugeno, M. Fuzzy identification of systems and its applications to modeling and control. *IEEE*
430 *Transactions On Systems Man And Cybernetics 1985*, 15, 116–132.
- 431 27. Martínez de la Casa Díaz, S. Human inspired humanoid robot control architecture. PhD thesis, University
432 Carlos III of Madrid, 2012.

433 **Sample Availability:** Samples of the compounds are available from the authors.

434 © 2017 by the authors. Submitted to *Sensors* for possible open access publication under the terms and conditions
435 of the Creative Commons Attribution (CC BY) license (<http://creativecommons.org/licenses/by/4.0/>).